Accepted for publication in the Astrophysical Journal

A Method for Deriving Accurate Gas-Phase Abundances for the Multiphase Interstellar Galactic Halo[1]

J. Christopher Howk[2,3], Kenneth R. Sembach[4], & Blair D. Savage[5]

ABSTRACT

We describe a new method for accurately determining total gas-phase abundances for the Galactic halo interstellar medium with minimal ionization uncertainties. For sight lines toward globular clusters containing both ultraviolet-bright stars and radio pulsars, it is possible to measure column densities of H I and several ionization states of selected metals using ultraviolet absorption line measurements and of H II using radio dispersion measurements. By measuring the ionized hydrogen column, we minimize ionization uncertainties that plague abundance measurements of Galactic halo gas. We apply this method for the first time to the sight line toward the globular cluster Messier 3 [$(l, b) = (42.^{\circ}2, +78.^{\circ}7)$; $d = 10.2$ kpc, $z = 10.0$ kpc] using *Far Ultraviolet Spectroscopic Explorer* and *Hubble Space Telescope* ultraviolet spectroscopy of the post-asymptotic giant branch star von Zeipel 1128 and radio observations by Ransom et al. of recently-discovered millisecond pulsars. The fraction of hydrogen associated with ionized gas along this sight line is $(45 \pm 5)\%$, with the warm ($T \sim 10^4$ K) and hot ($T \gtrsim 10^5$ K) ionized phases present in roughly a 5:1 ratio. This is the highest measured fraction of ionized hydrogen along a high-latitude pulsar sight line. We derive total gas-phase abundances $\log N(\mathrm{S})/N(\mathrm{H}) = -4.87 \pm 0.03$ and $\log N(\mathrm{Fe})/N(\mathrm{H}) = -5.27 \pm 0.05$. Our derived sulfur abundance is in excellent agreement with recent solar system determinations of Asplund, Grevesse, & Sauval.

[1]Based on observations with the NASA/ESA Hubble Space Telescope obtained at the Space Telescope Science Institute, which is operated by the Association of Universities for Research in Astronomy, Incorporated, under NASA contract NAS5-26555.

[2]Center for Astrophysics and Space Sciences, University of California, San Diego, C-0424, La Jolla, CA, 92093

[3]Current address: Department of Physics, University of Notre Dame, Notre Dame, IN 46556; jhowk@nd.edu

[4]Space Telescope Science Institute, Baltimore, MD, 21218; sembach@stsci.edu

[5]Astronomy Department, University of Wisconsin-Madison, Madison, WI, 53711; savage@astro.wisc.edu

However, it is -0.14 dex below the solar system abundance typically adopted in studies of the interstellar medium. The iron abundance is ~ -0.7 dex below the solar system abundance, consistent with the significant incorporation of iron into interstellar grains. Abundance estimates derived by simply comparing S II and Fe II to H I are +0.17 and +0.11 dex higher, respectively, than the abundance estimates derived from our refined approach. Ionization corrections to the gas-phase abundances measured in the standard way are, therefore, significant compared with the measurement uncertainties along this sight line. The systematic uncertainties associated with the uncertain contribution to the electron column density from ionized helium could raise these abundances by $\lesssim +0.03$ dex ($+7\%$). Uncertainties in the amount of very hot gas ($T \sim 10^6$ K) along the line of sight could also affect these determinations.

Subject headings: ISM: atoms – ISM: structure – ultraviolet: ISM

1. Introduction

Studies of gas-phase elemental abundances of the diffuse interstellar medium (ISM) of the Milky Way and other galaxies can give important information about dust composition, interstellar mixing, and chemical evolution. Most absorption line studies of gas associated with the warm neutral medium (WNM) of the Milky Way and other galaxies derive gas-phase abundances by comparing columns of the dominant ionization stage of a metal species in the WNM[1] with the column of neutral hydrogen, assuming (often implicitly) no ionization corrections are needed. Sight lines through the multiphase ISM of a galaxy not only probe neutral material, but often include gas associated with the warm ionized medium (WIM) and hot ionized medium (HIM). Ionized gas can represent up to $\sim 50\%$ of the total hydrogen column density for sight lines through the Galactic halo, with an average value of $\sim 25\%$ (Reynolds 1993). While the WIM likely contains very little H I, the dominant ionization states of many metals are the same for gas in the WNM and the WIM (e.g., S II, Fe II, Si II – see Sembach et al. 2000 and Haffner, Reynolds, & Tufte 1999). Thus, comparing the column densities of the dominant ionization states of metals to the column density of neutral hydrogen along a sight line will give apparent metal abundances that are too high compared with the true values. The neglect of ionization corrections may be a source of non-negligible systematic uncertainties to measurements of interstellar gas-phase abundances (Sembach et al. 2000; Howk & Sembach 1999).

[1]We refer to the dominant ionization states of elements in the warm neutral medium as "low ions." The dominant ionization stage of an element is typically the first whose ionization potential is higher than that of neutral hydrogen. We refer to the next higher ionization states as "intermediate ions."

In this paper we present a new approach for studying gas-phase abundances along extended paths through the multiphase halo of the Milky Way that circumvents such ionization uncertainties. Our strategy is to observe ultraviolet (UV) absorption lines from low and intermediate ions toward UV-bright stars in globular clusters that contain pulsars. This allows us to measure all of the ionization states of certain metals (e.g., sulfur and iron) present in the WNM and WIM in these directions. The total hydrogen column to which these metals are compared is the sum of the H I and H_2 column densities, derived from UV spectra, and the H II column density, determined using radio observations of the dispersion measures to the pulsars (which gives the electron column density). We present a full discussion of our methodology in §2.

We use this method to study the gas-phase abundances along the sight line toward the post-asymptotic giant branch star von Zeipel 1128 (vZ 1128) in the distant globular cluster Messier 3 (M 3). This sight line probes gas in the first 10 kpc above the Galactic plane. We discuss the UV absorption line and pulsar dispersion measure observations of this sight line in §3. The general properties of this interstellar sight line have previously been discussed by Howk, Sembach, & Savage (2003; hereafter Paper I). We also apply our new strategy for determining gas-phase abundances in this section, showing that the neglect of ionization corrections can lead to significant errors in the derived metal abundances along this (and presumably other) high-latitude sight lines. We end with a general discussion of the implications of this work in §4.

2. Methodology

In a multiphase medium, the total abundance, $A(X)$, of an element X with respect to hydrogen is

$$A(X) \equiv \frac{\sum_j N(X^j)}{N(\mathrm{H\ I}) + N(\mathrm{H\ II}) + 2N(\mathrm{H_2})}, \tag{1}$$

where $N(X^j)$ is the column density of the jth ionization stage of X. The numerator represents the total column density of the metal X, while the denominator is $N(\mathrm{H\ I}) + N(\mathrm{H\ II}) + 2N(\mathrm{H_2}) \equiv N(\mathrm{H})$, the total hydrogen column density. It is unusual that all the terms in both the numerator and the denominator can be measured. One approach is to identify special sight lines along which this is possible, such as those toward globular clusters that contain both UV-bright stars and radio pulsars.

The derivation of metal ion column densities is done using UV absorption line measurements against background sources (in our case against UV-bright stars) using the *Far Ultraviolet Spectroscopic Explorer* (*FUSE*) and/or the UV spectrographs on-board the *Hubble Space Telescope* (*HST*). A review of UV absorption line abundance techniques and measurements is given by Sav-

age & Sembach (1996). The transitions accessible to these instruments (with wavelength ranges of $912 \lesssim \lambda \lesssim 1187$ Å for *FUSE* and $1150 \lesssim \lambda \lesssim 3100$ Å for *HST*) limit the species for which we can reasonably approximate the total summation in the numerator of equation (1). Sulfur and iron are the only elements for which measurements are typically feasible for all of the ionization states expected to contribute significantly in the WNM and WIM (see Table 1 of Howk & Savage 1999 for a summary of WIM tracers). Measurements of gas associated with the HIM can also be made using absorption line spectroscopy of the O VI 1031.926 and 1037.617 Å doublet. However, it is not possible to measure the ions of S and Fe that dominate in the HIM. For example, the dominant ionization states of sulfur for $\log T \gtrsim 5.5$ are S VII and higher (Sutherland & Dopita 1993), which have no measurable UV transitions. We will make a correction (described below) for these still-unseen ions when deriving $A(X)$.

The neutral and molecular hydrogen column densities used in the denominator of equation (1) are also measured using UV absorption line techniques and instruments. H I column densities along sight lines to UV background sources are usually measured using the strong damping wings of the hydrogen Lyman-α transition at 1215.670 Å (e.g., Jenkins 1971; Bohlin, Savage, & Drake 1978; Diplas & Savage 1994). Measurements of H_2 are made using absorption lines of the Lyman and Werner electronic transitions in the *FUSE* bandpass (e.g., Savage et al. 1977; Shull et al. 2000).

We derive the H II column density from the radio dispersion measure, $DM = N(e^-) \equiv \int n_e dl$, observed toward pulsars in the target globular clusters. We make two corrections to the observed $N(e^-)$ in order to derive $N(\mathrm{H\ II})$ from $N(e^-)$: (1) a correction for the contribution to the electrons from ionized helium (the contribution from heavier elements is negligible); and (2) the removal of the contribution of the HIM, for which metal ions are typically not measurable.

The electron column in H+He gas is $N(e^-) = N(\mathrm{H\ II}) + N(\mathrm{He\ II}) + 2N(\mathrm{He\ III})$. We define the helium correction factor η such that $N(\mathrm{H\ II}) = \eta N(e^-)$. Therefore,

$$\eta \equiv \frac{1}{1 + A(\mathrm{He})x(\mathrm{He}^+)/x(\mathrm{H}^+) + 2A(\mathrm{He})x(\mathrm{He}^{+2})/x(\mathrm{H}^+)}, \tag{2}$$

where the ionization fraction of an ion X^j in the ionized gas is $x(X^j) \equiv N(X^j)/N(X)$. We assume $A(\mathrm{He}) = 0.1$ throughout. Values for η will typically be in the range 0.8 to 1.0.

Emission line studies of the WIM indicate $0.67 \lesssim x(\mathrm{H}^+)_{WIM} \lesssim 1.0$ (Reynolds 1989; Reynolds et al. 1998) and $x(\mathrm{He}^+)_{WIM} \lesssim 0.27\, x(\mathrm{H}^+)_{WIM}$ (Reynolds & Tufte 1995). Most photoionization models of the WIM predict $x(\mathrm{He}^{+2})_{WIM}$ to be very small (Sembach et al. 2000; Mathis 2000), giving values of η_{WIM} near 1.0. However, Arabadjis & Bregman (1999) suggest $x(\mathrm{He}^{+2})_{WIM}$ is non-negligible on the basis of X-ray absorption estimates (although see Slavin, McKee, & Hollenbach 2000 for alternative interpretations of these data). In what follows, we consider two cases: $x(\mathrm{He}^{+2})_{WIM} \approx 0$ and $x(\mathrm{He}^{+2})_{WIM} = 1 - x(\mathrm{He}^+)_{WIM}$; we refer to these as the

minimum and maximum helium ionization cases, respectively, and tabulate characteristic values of η in Table 1. We favor the minimum helium ionization model given that much of the sulfur in the WIM is in the form of S II (Haffner et al. 1999), implying the ionization state of metals in the WIM is relatively low.

It is extremely difficult to measure the dominant metal ionization states in the HIM. We therefore subtract an estimated HIM contribution, $N(e^-)_{HIM}$, from $N(e^-)$ to derive a value of $N(\mathrm{H\ II})$ appropriate for the WIM alone. We use measurements of O VI to estimate $N(e^-)_{HIM}$, adopting the following two-component prescription:

$$N(e^-)_{HIM} = \frac{1}{\eta_{HIM}} \left[\frac{N(\mathrm{O\ VI})}{A(\mathrm{O}) x(\mathrm{O}^{+5})} + \langle n_{\mathrm{H}} \rangle_c \, d \right], \tag{3}$$

where $N(\mathrm{O\ VI})$ is the measured O VI column density, and d is the distance of the globular cluster from the sun. The first term in brackets is the column density of $T \sim 3 \times 10^5$ K gas associated with the thick disk distribution of the Milky Way, which is best probed by O VI (Wakker et al. 2003; Savage et al. 2003). The second term accounts for an extended hot corona assumed to be uniformly distributed and characterized by $T \gtrsim 10^6$ K and a total hydrogen density $\langle n_{\mathrm{H}} \rangle_c \sim 2 \times 10^{-4}$ cm^{-3}. The existence of this component is derived from observations of O VI associated with high-velocity clouds, which suggest these clouds are interacting with a hot, low-density plasma extending to large distances (> 70 kpc) from the Sun (Sembach et al. 2003). Supporting evidence for a hot corona is provided by very strong zero redshift X-ray absorption lines of Ne IX, O VII and O VIII in the spectra of X-ray bright active galaxies (Nicastro et al. 2002; Fang et al. 2003; Rasmussen, Kahn, & Paerels 2003) and Galactic X-ray sources (Futamoto et al. 2004; Yao & Wang 2005).

Defining the WIM electron column as $N(e^-)_{WIM} = N(e^-) - N(e^-)_{HIM}$, i.e., correcting for the contribution from the HIM, we rewrite Eqn. (1) as

$$A(X) = \frac{\sum\limits_{j(WNM,WIM)} N(X^j)}{[N(\mathrm{H\ I}) + \eta_{WIM} N(e^-)_{WIM} + 2N(\mathrm{H_2})]}, \tag{4}$$

noting the summation is over metal ionization states found in the WNM and WIM (i.e., excluding the HIM). We suggest using numerical values for the minimum and maximum helium ionization cases of $\eta_{WIM} = 0.98 \pm 0.01$ and 0.81 ± 0.04, where the uncertainties correspond to the dispersion of values found in Table 1.

The differences in the helium ionization assumptions represent the dominant source of systematic uncertainty in our method. The magnitude of the uncertainty is roughly $0.2 \times N(\mathrm{H\ II})_{WIM}/N(\mathrm{H})$, or $\lesssim 10\%$ for high-latitude sight lines. While spatial variations of $N(e^-)$ between the sight lines to the M 3 pulsars and the UV bright stars could be another potential source of systematic uncertainty, it seems in most cases this effect is negligible. For example, Freire et al. (2001) find the dispersion

in the DM values toward 15 pulsars in 47 Tuc is only 0.5% of the average with a full range of $\approx 2\%$ of the average (for pulsars with a maximum angular separation of $\approx 2'$).

3. Application to the Sight Line Toward von Zeipel 1128 in Messier 3

We now apply the approach outlined above to determine average gas-phase abundances of sulfur and iron in the WNM and WIM toward the high-latitude globular cluster M 3 [$(l, b) = (42.^{\circ}2, +78.^{\circ}7)$; $d = 10.2$ kpc, $z = 10.0$ kpc]. We describe in the following subsections the UV data and analysis that are used to derive the metal and neutral hydrogen column densities, the radio observations used to derive the electron column density toward M 3, and the resulting analysis of the total abundances of S and Fe in this direction.

3.1. UV Absorption Line Measurements of Metals and Neutral Hydrogen

In Paper I we presented UV absorption line measurements of the ISM in the direction of vZ 1128. That work was based upon *FUSE* observations covering the spectral range 905–1187 Å with a resolution of ~ 20 km s^{-1}. In this work we present new observations of vZ 1128 obtained with the Space Telescope Imaging Spectrograph (STIS) on board *HST* under guest observer proposal GO 9150. Proffitt et al. (2001) discuss the detailed characteristics of this instrument.

The properties of our STIS observations of vZ 1128 are summarized in Table 2. A total of 12.7 ksec of exposure time was collected with each of the E140M and E230M intermediate resolution echelle gratings. These data have signal-to-noise ratios varying from ~ 10 to 20 per resolution element. The shorter wavelength E140M grating observations have a resolution of ~ 6.5 km s^{-1} (FWHM), while the longer wavelength E230M observations have a resolution ~ 10 km s^{-1} (FWHM). All observations were made through the $0.''2 \times 0.''06$ apertures. The STIS data were calibrated using v2.17 of the CALSTIS pipeline.

We use the STIS data to derive column densities and limits for the species H I, S I, S II, and Fe I. The details of our measurements of metal line and H I column densities are presented below. We do not make use of the longest-wavelength E230M exposure (archive ID O6F501030). An analysis of the full STIS spectrum will be presented in a future work.

3.1.1. H I *Column Density from Lyman-*α

We derive the interstellar H I column density of the vZ 1128 sight line by fitting the damping wings of the Lyman-α profile. We generally follow the procedures described by Sonneborn et al. (2002) for determining the H I column density and uncertainty.

Figure 1 shows the STIS spectrum of the Lyman-α absorption line toward vZ 1128. This absorption line contains contributions from both the stellar atmosphere of vZ 1128 and the ISM in this direction. We use a model stellar atmosphere to normalize the data during the fitting process. Our adopted atmosphere, kindly provided by P. Chayer (2002, private communication), was calculated using the SYNSPEC package of I. Hubeny (2000, private communication) and assumed $T_{eff} = 35,000$ K, $\log g = 4.0$, and He/H $= 0.1$ (Dixon, Davidsen, & Ferguson 1994). The adopted atmosphere is shown as the blue line in Figure 1. We adopt a second-order Legendre polynomial correction to the model atmosphere to match it to the STIS spectrum, following Sonneborn et al. (2002). This is done to account for any calibration and order combination uncertainties in the data or any uncertainties in the large-scale flux distribution of the models. The parameters of the polynomial are allowed to vary during the fitting process.

The interstellar column density that best fits the STIS observations of Lyman-α is $\log N(\mathrm{H\ I}) = 19.98 \pm 0.03$. This is slightly different (0.01 dex higher) than the value quoted in Paper I and is due to a better calibration and combination of the data. The best-fit profile is shown as the red line in Figure 1. Our error estimate includes contributions from the uncertainties in the adopted properties of the stellar model (c.f., Sonneborn et al. 2002), which dominate the total error budget.

Two observations of the H I 21 cm emission line in this direction give slightly higher column density estimates (as discussed in Paper I). Danly et al. (1992) collected H I 21 cm emission line observations toward vZ 1128 using the NRAO Green Bank 140-ft. telescope, which has a beam of $21'$. The Leiden-Dwingeloo Survey (LDS; Hartmann & Burton 1997), which has a beam size of $35'$, includes a pointing centered $\approx 12'$ from vZ 1128. Table 3 gives the H I column densities in the direction of M 3/vZ 1128 derived from the two 21-cm observations and the Lyman-α profile. The NRAO and first LDS value were derived here through a direct integration of the brightness temperature distribution over the range $-75 \leq v_{\mathrm{LSR}} \leq +75$ km s^{-1} in the optically-thin limit (optical depth effects are $< 1\%$ for this high-latitude sight line). The second LDS H I value is from Wakker et al. (2003); it is the sum of three Gaussians fit to a weighted average of four LDS pointings in this direction. The difference in column densities between these two treatments of the LDS data is likely due to the slightly different spectra adopted (a single pointing versus a weighted average of four pointings) and the different techniques used to derive column densities (a direct integration versus Gaussian fits). Both the Danly et al. (1992) and LDS observations have been corrected for stray radiation. The uncertainties given in Table 3 do not include contributions from errors in this correction. Lockman & Savage (1995) estimate the stray radiation correction

uncertainty of observations similar to those of Danly et al. (1992) to be of order $\sigma[N(\mathrm{H\ I})] \sim 10^{19}$ cm^{-2}, or ~ 0.04 dex for the column densities in Table 3.

All of the H I columns derived using 21-cm observations are higher than that derived above via a direct fit to Lyman-α absorption toward vZ 1128. The largest difference is 0.08 dex, or 20%, between the NRAO spectrum and the fit to Lyman-α. This difference is likely due to structure in the H I column on scales smaller than the 21 cm beam (see Savage et al. 2000), although it could also be caused by systematic effects (e.g., unaccounted for uncertainties in the adopted stellar Lyman-α profile or uncertainties in the 21 cm stray radiation correction). In Figure 1 we show the best-fit Lyman-α profile if we assume $\log N(\mathrm{H\ I}) = 20.06$ as the green line. The polynomial continuum correction is allowed to vary when fitting this profile to the data. This column over-predicts the optical depth in the wings of Lyman-α. In what follows, we assume the Lyman-α profile provides the best estimate of $N(\mathrm{H\ I})$ in this direction.

3.1.2. Metal Line Column Densities

We have used the new STIS data to derive column densities and limits for the metal species S I, S II, and Fe I. Our measurements of the metal line properties toward vZ 1128 follow Paper I. We have fit the stellar continuum in the regions surrounding metal transitions using low order Legendre polynomials. Following Sembach & Savage (1992), we have directly integrated the observed line profiles and apparent optical depths to arrive at the equivalent widths and apparent column densities, N_a (Savage & Sembach 1992). These measurements are presented in Table 4. We also list our adopted central wavelengths and oscillator strengths (all from Morton 2003) for the transitions, the velocity range over which the interstellar absorption lines were integrated, and an empirical estimate of the signal to noise ratio per resolution element in the region about each line. The quoted measurement errors include contributions from continuum placement uncertainties and the effects of a 2% error in the flux zero level (c.f., Sembach & Savage 1992).

Of the metal species considered in this work, only S II is detected in the STIS data. The absorption line profiles of the S II triplet at 1250.584, 1253.811, and 1259.519 Å from STIS E140M observations of vZ 1128 are shown in Figure 2; also shown is the profile of the S III 1012.495 Å line from the *FUSE* observations of this star (Paper I). To calculate the limiting equivalent widths and apparent column densities of S I and Fe I, we assume the gas traced by these species has an intrinsic width of ~ 40 km s^{-1} (FWHM), which is the value derived from a single Gaussian profile fit to the S II 1250.584 Å transition. All limits given in this work are 3σ.

The integrated apparent column densities of the weaker two transitions at 1250.584 and 1253.811 Å, which have f-values that are different by a factor of two, differ by ~ 0.01 dex,

with the weaker transition giving a higher N_a. The strongest line, with an f-value three times that of the weakest, gives a value of N_a that is -0.05 dex lower than the weakest line. The progression of decreasing N_a with increasing f suggests these lines may contain unresolved saturated structure (Savage & Sembach 1991).

Figure 3 shows a comparison of the apparent column density profiles as a function of velocity, $N_a(v)$, for the three transitions. In each of the panels, the weakest S II transition at 1250.584 Å is shown as the thin black histogram, while the two stronger transitions are plotted as thick gray histograms. The $N_a(v)$ profiles in Figure 3 do not show the classical symptoms of unresolved saturated structure, with the highest peaks of the strong line profiles suppressed compared with the weak line profiles. The central dip near $v_{\rm LSR} \approx -20$ km s^{-1} in the S II 1259 Å profile may be indicating the presence of a blended, but saturated, component at these velocities.

Because of the possible presence of saturated structure in these profiles, we apply a correction to the data following the methodology outlined in Savage & Sembach (1991). We derive this correction separately for the line pairs $\lambda1250$+$\lambda1253$ and $\lambda1253$+$\lambda1259$ and average the results. Our adopted total column density is $\log N({\rm S\ II}) = 15.28 \pm 0.02$. Independent support for this column density comes from a curve of growth analysis. A single component curve of growth fit to the equivalent widths of these three transitions gives $\log N({\rm S\ II}) = 15.28^{+0.03}_{-0.02}$ for a Doppler parameter of $b = 19.5 \pm 1.2$ km s^{-1}.

Table 5 lists the final column densities adopted in this work, including those of S III, Fe II, Fe III, and O VI and of the limits to H_2, S IV, and S VI from our analysis of the *FUSE* data in Paper I.

3.2. Pulsar Dispersion Measurements and the Electron Column Density

3.2.1. Radio Pulsar Dispersion Measurements

The electron column density toward M 3 is derived from the dispersion measures determined by Ransom et al. (2004) for three binary millisecond pulsars in M 3. These pulsars were discovered with the Arecibo 305-m radio telescope at 20 cm using the Wideband Arecibo Pulsar Processors and the search algorithms described by Ransom, Cordes, & Eikenberry (2003) and Ransom, Eikenberry, & Middleditch (2002).

The average dispersion measure toward the three pulsars M 3A, M 3B, and M 3D is $DM = 26.33 \pm 0.15$ pc cm^{-3} (standard deviation). We do not include the unconfirmed pulsar M 3C in this average, although it gives a consistent DM (Ransom et al. 2004). Typical uncertainties in the individual measurements are ~ 0.1 pc cm^{-3}. The average dispersion measure corresponds to

an electron column density of $\log N(e^-) = 19.912 \pm 0.002$. This is the total electron column, including contributions from the WIM and the HIM along this sight line.

3.2.2. Correcting for the Hot ISM

Applying equation (3) to the 10 kpc sight line toward vZ 1128 (Paper I), which is very close to the north Galactic pole, yields $N(e^-)_{HIM} \sim 1.2 \times 10^{19}$ cm^{-2}. This estimate assumes an interstellar gas-phase abundance $A(\mathrm{O}) = 4.08 \times 10^{-4}$ (André et al. 2003), an ionization fraction $x(\mathrm{O}^{+5}) = 0.2$ (Sutherland & Dopita 1993; see Savage et al. 2003), and an O VI column $N(\mathrm{O\ VI}) = 3.1 \times 10^{14}$ cm^{-2} (Paper I). We adopt $\langle n_{\mathrm{H}} \rangle_c \sim 2 \times 10^{-4}$ cm^{-3} as the coronal density for the second term in brackets in equation (3). We have assumed a medium with fully-ionized hydrogen and helium, $\eta_{HIM} = 0.83$.

We will adopt a 50% uncertainty in calculations of the HIM column using the parameters for equation (3) adopted above. We have assumed $x(\mathrm{O}^{+5})$ equal to its maximum in collisional ionization equilibrium models (Sutherland & Dopita 1993). While much of the O VI may in fact reside in regions where $x(\mathrm{O}^{+5}) \approx 0.2$, the O VI ionization fraction in the transition temperature gas along extended sight lines through the thick disk of the Galaxy is uncertain. We've assumed a single, constant density component for the 10^6 K material in an effort to approximate a Galactic corona. Yao & Wang (2005) have estimated the density distribution of this hot component of the ISM using X-ray absorption measurements of Ne IX, O VII and O VIII toward several Galactic targets, mostly in the Galactic Center region. They present two model density distributions based on their data: a plane-parallel, exponential disk distribution and a spherical distribution about the Galactic Center. These models give estimates of $N(e^-)_{HIM} \sim 2.9 \times 10^{19}$ cm^{-2} and $\sim 1.2 \times 10^{19}$ cm^{-2}, respectively, for the sight line to vZ 1128 (with uncertainties > 30 to 50%). However, these results are likely to be strongly influenced by hot gas in the inner Galaxy. It is not clear that the Yao & Wang density distributions are appropriate for the hot ISM at the solar circle. We will adopt the predictions of equation (3) as calculated in the preceding paragraph for the HIM column and assume a 50% uncertainty.

3.3. Total Abundances

Table 6 summarizes the results of our analysis of the M 3 sight line, following the method described in §2. The total column density of sulfur toward vZ 1128 is $\log N(\mathrm{S}) = 15.34 \pm 0.02$; the contributions from S I, S IV and S VI are negligible [with combined 3σ limits less than a few percent of $N(\mathrm{S})$]. The total column of iron is $\log N(\mathrm{Fe}) = 14.95 \pm 0.04$, where we have assumed

the contributions from Fe IV and higher ionization states in WNM and WIM gas are negligible (as they are for ions of sulfur).

In Table 6 we include the values of $A(\mathrm{S})$ and $A(\mathrm{Fe})$ for both the minimum and maximum helium ionization assumptions. We give the values adopted for the helium correction, η_{WIM} and the values of $N(e^-)$ associated with the WIM and the HIM. Also included in Table 6 are the column of hydrogen (neutral+ionized) and the fraction of hydrogen found in the ionized phase. Those values with a "Total" subscript refer to measurements that include the contribution from the HIM. Thus, the hydrogen column $N(\mathrm{H})_{Total}$ includes contributions from the WNM, WIM, and HIM, whereas $N(\mathrm{H})$ includes contributions from the WNM and WIM only. As stated above, the reason for this distinction is that we have not measured metals associated with the hot phase with the exception of O VI.

4. Discussion and Conclusions

We have derived the average gas-phase interstellar abundances in a way that minimizes ionization uncertainties along the sight line to the halo globular cluster M 3. The abundance of sulfur toward M 3 is $\log A(S) = -4.87 \pm 0.03$. Because sulfur is not believed to be significantly incorporated into dust grains, $A(\mathrm{S})$ represents the total average metal abundance of the neutral and ionized ISM along this sight line. The sight line to M 3 probes warm material associated with the thin interstellar disk and the extended (thick disk) distribution of neutral and ionized gas (Paper I).

Typically, the solar system abundance for sulfur adopted by ISM studies is $\log A(\mathrm{S})_\odot = -4.73$ (Savage & Sembach 1996), an average of the discrepant photospheric, $\log A(\mathrm{S})_\odot = -4.67 \pm 0.11$, and meteoritic, $\log A(\mathrm{S})_\odot = -4.80 \pm 0.06$, values from Grevesse & Sauval (1998). Thus, our total sulfur abundance along the sight line to M 3 is -0.14 ± 0.03 dex below, or $\sim 3/4$ of, the commonly-adopted solar value.[2] Recent revisions to the solar composition, however, are in very good agreement with our new measurement. Asplund, Grevesse, & Sauval (2005) derive $\log A(\mathrm{S})_\odot = -4.86 \pm 0.05$ for the solar photosphere, while incorporating the meteoritic data from Lodders (2003) with their results gives a meteoritic abundance of $\log A(\mathrm{S})_\odot = -4.84 \pm 0.04$.[3] It is somewhat disconcerting for ISM studies that the recommended solar abundances are in such a state of flux. However, the excellent agreement between our determination of $A(S)$ toward vZ 1128 and

[2]In the remaining discussion we adopt the results of the minimum helium ionization case, our preferred model. For simplicity we do not explicitly refer to the ~ 0.03 dex systematic uncertainty associated with this choice of model.

[3]Because H is deficient in meteorites, the metal abundances in meteorites are derived relative to Si. The absolute meteoritic abundances are then calculated from an adopted solar photospheric Si/H ratio. In this case, Asplund et al. (2005) use $\log A(\mathrm{Si})_\odot = 7.51 \pm 0.04$.

the most recent solar system estimates is encouraging.

In contrast to sulfur, iron is heavily incorporated into grains. Our iron abundance measurement is $\log A(\mathrm{Fe}) = -5.26 \pm 0.04$. Most of the difference between the gas-phase interstellar abundance and the solar system abundance, $\log A(\mathrm{Fe})_{\odot} = -4.55 \pm 0.03$ (Asplund et al. 2005), is due to the incorporation of Fe into dust in both the WNM and WIM.

The ratio of sulfur to hydrogen derived in the usual way toward vZ 1128 is $\log N(\mathrm{S\ II})/N(\mathrm{H\ I}) = -4.70 \pm 0.04$, consistent with the Grevesse & Sauval (1998) solar system value and $+0.17$ dex higher than the total abundance derived above using our method of correcting for ionized gas contributions. The neglect of ionization corrections causes a systematic error that is significantly higher than the estimated statistical uncertainties. Similarly, we derive $\log N(\mathrm{Fe\ II})/N(\mathrm{H\ I}) = -5.18 \pm 0.06$, implying a systematic error of $+0.09$ dex. The abundances derived by comparing singly-ionized sulfur and iron with H I both overestimate the true gas-phase abundances by significant amounts. We note that although the direct comparison of two singly-ionized species reduces the impact of ionization uncertainties, they are still not negligible compared with typical statistical uncertainties. For the sight line toward M 3 we find $\log N(\mathrm{Fe})/N(\mathrm{S}) = -0.40 \pm 0.05$, while simply comparing the column densities of singly-ionized atoms gives $\log N(\mathrm{Fe\ II})/N(\mathrm{S\ II}) = -0.48 \pm 0.05$. For comparison, the solar system ratio from Asplund et al. (2005) is $\log N(\mathrm{Fe})/N(\mathrm{S}) = +0.31$, while the standardly-adopted value in ISM studies has been +0.23 (see Savage & Sembach 1996).

The overestimate of gas-phase abundances derived by comparing singly-ionized species with neutral hydrogen is not unique to this sight line. While the fraction $N(\mathrm{H\ II})_{Total}/N(\mathrm{H})_{Total} \approx 0.45 \pm 0.04$ for the vZ 1128 sight line is the highest yet reported (Reynolds 1993), the WIM will contribute to the singly-ionized metal column densities along all high-latitude sight lines. Several groups have derived near-solar abundances of sulfur comparing S II with H I along high-latitude sight lines with H I column densities similar to that toward vZ 1128 in M 3 (e.g., Howk et al. 1999; Spitzer & Fitzpatrick 1993). It is likely that the abundances derived in these studies suffer from the systematic effects of ionized gas as well.

It may be possible to model the contribution from the ionized gas along a sight line and correct for its systematic effects on abundance studies. Using the WIM models constructed by Domgörgen & Mathis (1994), Sembach & Savage (1996) estimated that the magnitude of ionization uncertainties for derived gas-phase elemental abundances should be less than ~ 0.1 to 0.2 dex along most sight lines through the Galactic halo, consistent with the values derived in this work.

Unless $A(\mathrm{S})$ varies significantly within the Galaxy, however, correcting for ionization effects may not be so straightforward. Howk et al. (1999), in their detailed study of the sight line to μ Columbae, derived $\log N(\mathrm{S\ II})/N(\mathrm{H\ I}) = -4.65 \pm 0.02$; they used photoionization models to

argue that the sulfur abundance along this sight line was near their adopted solar system value of $\log A(\mathrm{S})_{\odot} = -4.73$ (as recommended by Savage & Sembach 1996). In this case, the star is much closer to the Sun than vZ 1128, and Howk et al. assumed an H II region about the star dominated the ionized gas content of the sight line. Even adopting the maximum ionization correction derived by Howk et al. (1999), however, gives a sulfur abundance ≈ 0.2 dex higher than that derived toward vZ 1128 in this work.

Sembach et al. (2000) produced detailed models for the ionization of the WIM by OB stars and used the models to estimate the ionization corrections required for the sight line to the distant halo star HD 93521 (Spitzer & Fitzpatrick 1993). Their models predict an ionization correction of ≈ -0.2 dex to $A(\mathrm{S})$ derived by Spitzer & Fitzpatrick (1993), giving $A(\mathrm{S})$ consistent with that derived in this work. However, applying their method to the sight line toward vZ 1128 yields an abundance $\log A(\mathrm{S}) = -5.3$, or ≈ -0.4 dex from the value derived in this work.

These examples call into question our ability to effectively model the effects of WIM gas more generally. Indeed, models designed to match emission line diagnostics may not be good descriptors of the absorption line diagnostics of the WIM, which are more sensitive to low-density gas.

We can state with confidence that abundance studies of almost all high-latitude, low hydrogen column density [$\log N(\mathrm{H\ I}) \lesssim 20$] sight lines are affected by the presence of ionized gas when comparing singly-ionized metal species with H I. The degree to which an individual sight line is contaminated likely depends on the fraction of hydrogen along the sight line that is ionized. The work of Reynolds (1993) suggests that this fraction can range from $\sim 20\%$ to $\sim 50\%$. We note that some species can be reliably compared if they have similar ionization properties; for example, the ratio O I/H I should not be affected by ionization effects like those discussed here given the strong charge exchange reaction that locks the ionization state of these species together. Unfortunately, the far-UV O I lines toward vZ 1128 are strongly saturated while the weak O I 1355 Å transition is not detected.

We will apply the technique outlined here to more sight lines and to an extended array of metal species in the future to study this source of systematic uncertainties in regions of varying physical conditions and fractional ionization. At least three other globular clusters contain both radio pulsars and stars with sufficient UV flux to allow measurements like those presented in this work.

We thank S. Ransom for discussions regarding the dispersion measures toward pulsars in M 3. Support for proposal numbers HST-GO-9150.03-A and HST-GO-9410.03-A was provided by NASA through grants from the Space Telescope Science Institute, which is operated by the

Association of Universities for Research in Astronomy, Incorporated, under NASA contract NAS5-26555. K.R.S. acknowledges support from NASA contract NAS5-32985 to the Space Telescope Science Institute.

REFERENCES

André, M., et al. 2003, ApJ, 591, 1000

Arabadjis, J.S., & Bregman, J.N. 1999, ApJ, 510, 806

Asplund, M., Grevesse, N., & Sauval, A.J. 2005, in ASP Conf. Ser. 336, Cosmic Abundances as Records of Stellar Evolution and Nucleosynthesis, ed. F.N. Bash, & T.G. Barnes, (San Francisco: ASP), 25

Bohlin, R.C., Savage, B.D., & Drake, J.F. 1978, ApJ, 224, 132

Diplas, A., & Savage, B.D. 1994, ApJS, 93, 211

Dixon, W.V., Davidsen, A.F., & Ferguson, H.C. 1994, AJ, 107, 1388

Domgörgen, H., & Mathis, J.S. 1994, ApJ, 428, 647

Fang, T., Sembach, K.R., & Canizares, C.R. 2003, ApJ, 586, L49

Freire, P.C., Kramer, M., Lyne, A.G., Camilo, F., Manchester, R.N., & D'Amico, N. 2001, ApJ, 557, L105

Futamoto, K., Mitsuda, K., Takei, Y., Fujimoto, R., & Yamasaki, N.Y. 2004, ApJ, 605, 793

Gómez, G.C., Benjamin, R.A., & Cox, D.P. 2001, ApJ, 122, 908

Grevesse, N., & Sauval, A.J. 1998, SSRv, 85, 161

Haffner, L.M., Reynolds, R.J., & Tufte, S.L. 1999, ApJ, 523, 223

Hartmann, D., & Burton, W.B. 1997, Atlas of Galactic Neutral Hydrogen, (Cambridge: Cambridge Univ. Press)

Howk, J.C., & Savage, B.D. 1999, ApJ, 517, 746

Howk, J.C., Savage, B.D., & Fabian, D. 1999, ApJ, 525, 253

Howk, J.C., Savage, B.D., Sembach, K.R., & Hoopes, C.G. 2002, ApJ, 572, 264

Howk, J.C., & Sembach, K.R. 1999, ApJ, 523, L141

Howk, J.C., Sembach, K.R., & Savage, B.D. 2003, ApJ, 586, 249 (Paper I)

Jenkins, E.B. 1971, ApJ, 169, 25

Lockman, F.J., & Savage, B.D. 1995, ApJS, 97, 1

Lodders, K. 2003, ApJ, 591, 1220

Mathis, J.S. 2000, ApJ, 544, 347

Meyer, D.M., Jura, M., & Cardelli, J.A. 1998, ApJ, 493, 222

Nicastro, F., et al. 2002, ApJ, 573, 157

Proffitt, C., et al. 2002, "STIS Instrument Handbook", Version 6.0, (Baltimore: STScI)

Ransom, S.M., et al. 2004, in Binary Radio Pulsars, eds. F. Rasio & I.Stairs, in press (astro-ph/0404213)

Ransom, S.M., Cordes, J.M., & Eikenberry, S.S. 2003, ApJ, 589, 911

Ransom, S.M., Eikenberry, S.S., & Middleditch, J. 2002, AJ, 124, 1788

Rasmussen, A., Kahn, S.M., & Paerels, F. 2003, in The IGM/Galaxy Connection: The Distribution of Baryons at $z = 0$, ed. J.L. Rosenberg & M.E. Putman (Dordrecht: Kluwer), 109

Reynolds, R.J. 1989, ApJ, 345, 811

Reynolds, R.J. 1993, in Back to the Galaxy, ed. S. Holt & F. Verter (New York: American Institute of Physics), 156

Reynolds, R.J., & Tufte, S.L. 1995, ApJ, 439, L17

Reynolds, R.J., Hausen, N.R., Tufte, S.L., & Haffner, L.M. 1998, ApJ, 494, L99

Savage, B.D., et al. 2000, ApJS, 129, 563

Savage, B.D., Drake, J.F., Budich, W., & Bohlin, R.C. 1977, ApJ, 216, 291

Savage, B.D., & Sembach, K.R. 1996, ARA&A, 34, 279

Savage, B.D., & Sembach, K.R. 1991, ApJ, 379, 245

Savage, B.D., et al. 2003, ApJS, 146, 125

Sembach, K.R., et al. 2003, ApJS, 146, 165

Sembach, K.R., Howk, J.C., Ryans, R.S.I., & Keenan, F.P. 2000, ApJ, 528, 310

Sembach, K.R., & Savage, B.D. 1992, ApJS, 83, 147

Shull, J.M., et al. 2000, ApJ, 538, 73

Slavin, J.D., McKee, C.F., & Hollenbach, D.J. 2000, ApJ, 541, 218

Spitzer, L., & Fitzpatrick, E.L. 1993, ApJ, 409, 299

Sutherland, R.S., & Dopita, M.A. 1993, ApJS, 88, 253

Wakker, B.P., et al. 2003, ApJS, 146, 1

Wakker, B.P., Kalberla, P.M.W., van Woerden, H., de Boer, K.S., & Putman, M.E. 2001, ApJS, 136, 537

Yao, Y., & Wang, Q.D. 2005, ApJ, 624, 751

Table 1. Values of Helium Correction Factor η

$x(\mathrm{H}^+)$	$x(\mathrm{He}^+)/x(\mathrm{H}^+)$	$x(\mathrm{He}^{+2})$	η
Minimum Helium Ionization[a]			
0.67	0.15	0.00	0.99
0.80	0.15	0.00	0.99
1.00	0.15	0.00	0.99
0.67	0.27	0.00	0.97
0.80	0.27	0.00	0.97
1.00	0.27	0.00	0.97
Maximum Helium Ionization[b]			
0.67	0.00	1.00	0.77
0.80	0.00	1.00	0.80
1.00	0.00	1.00	0.83 [c]
0.67	0.15	0.78	0.80
0.80	0.15	0.81	0.82
1.00	0.15	0.85	0.84
0.67	0.27	0.60	0.83
0.80	0.27	0.66	0.84
1.00	0.27	0.73	0.85

[a]The minimum helium ionization case assumes $x(\mathrm{He}^{+2}) = 0$.

[b]The maximum helium ionization case assumes $x(\mathrm{He}^{+2}) = 1 - x(\mathrm{He}^+)$.

[c]This case is appropriate for HIM gas.

Table 2. STIS Observations of vZ 1128[a]

Archive ID	Grating	t_exp [ksec]	$R \equiv \lambda/\Delta\lambda$	FWHM [km/s]	λ Range [Å]
O6F502010	E140M	2.0	45000	6.5	1140–1735
O6F502020	E140M	10.7	45000	6.5	1140–1735
O6F501010	E230M	2.0	30000	10	1575–2380
O6F501020	E230M	8.0	30000	10	1575–2380
O6F501030	E230M	2.7	30000	10	2305–3110

[a]All observations were taken through the $0\farcs2 \times 0\farcs06$ apertures on 2002 August 16-17.

Table 3. H I Observations in the Direction of vZ 1128

Source	Beam	$\log N$(H I)[a]	Source[b]
NRAO 21 cm	21′	20.058 ± 0.003	1
LDS 21 cm	35′	20.044 ± 0.005	1
LDS 21 cm	35′	20.017 ± 0.006	2
STIS Lyman-α	···	19.98 ± 0.03	3

[a]The uncertainties quoted for the 21 cm observations do not contain a contribution from errors in the stray radiation or baseline corrections. These are likely of order 0.04 dex for this sight line.

[b]Sources: (1) This work, through direct integration of the brightness temperature profile; (2) Wakker et al. 2003 through a Gaussian decomposition of the profile; (3) This work, through a fit to the Lyman-α profile (see text).

Table 4. Selected Interstellar Absorption Line Measurements toward vZ 1128[a]

Species	λ_c [Å][b]	$\log \lambda f$[c]	v_-, v_+[d]	W_λ [mÅ]	$\log N_a$	S/N
S I	1425.030	2.437	$\cdots$	< 15	< 12.7	16
S II	1250.584	0.834	$-50, 35$	102 ± 4	15.25 ± 0.02	19
S II	1253.811	1.135	$-75, 35$	162 ± 5	15.24 ± 0.02	19
S II	1259.519	1.311	$-75, 35$	190 ± 6	15.20 ± 0.03	15
Fe I	2167.453	2.512	$\cdots$	< 21	< 12.5	18

[a]Measurements from STIS E140M and E230M observations of vZ 1128. All limits are 3σ and uncertainties include contributions from photon statistics and an assumed zero-point uncertainty of 2% of the local continuum. Signal-to-noise ratios, S/N, determined empirically following Sembach & Savage 1992.

[b]Rest wavelength of the transition, from the compilation of Morton 2003.

[c]Oscillator strength, f, given as $\log \lambda f$, from the compilation of Morton 2003.

[d]LSR velocity range of integration for quoted values of equivalent width and apparent column density.

Table 5. Adopted Column Densities Toward M 3

Species	$\log N$	Ref.[a]
H I	19.98 ± 0.03	1
e^-	19.912 ± 0.002	2
H_2	$< 14.35\,(3\sigma)$	1
O VI	14.49 ± 0.03	1
S I	$< 12.7\,(3\sigma)$	3
S II	15.28 ± 0.02	3
S III	14.47 ± 0.03	1
S IV	$< 13.7\,(3\sigma)$	1
S VI	$< 13.4\,(3\sigma)$	1
Fe I	$< 12.5\,(3\sigma)$	3
Fe II	14.80 ± 0.05	1
Fe III	14.42 ± 0.05	1

[a]References: (1) Howk et al. 2003 (Paper I); (2) Ransom et al. 2004; (3) this work.

Table 6. Derived Interstellar Parameters Toward M 3

Quantity	Helium Ionization	
	Minimum[a]	Maximum[b]
η_{WIM} [c]	0.98 ± 0.01	0.81 ± 0.04
$\log N(e^-)$	19.912 ± 0.002	
$\log N(e^-)_{HIM}$	19.10 ± 0.12	
$\log N(e^-)_{WIM}$	19.84 ± 0.03	
$\log N(\mathrm{H\ II})_{HIM}$	19.01 ± 0.18	
$\log N(\mathrm{H\ II})_{WIM}$	19.83 ± 0.04	19.75 ± 0.04
$\log N(\mathrm{H})$[d]	20.22 ± 0.02	20.19 ± 0.03
$\log N(\mathrm{H})_{Total}$[e]	20.24 ± 0.03	20.21 ± 0.03
$N(\mathrm{H\ II})_{WIM}/N(\mathrm{H})$[d]	0.42 ± 0.04	0.37 ± 0.04
$N(\mathrm{H\ II})_{Total}/N(\mathrm{H})_{Total}$[e]	0.45 ± 0.05	0.41 ± 0.06
$\log N(\mathrm{S})$	15.34 ± 0.02	
$\log N(\mathrm{Fe})$	14.95 ± 0.04	
$\log A(\mathrm{S})$	-4.87 ± 0.03	-4.84 ± 0.03
$\log A(\mathrm{Fe})$	-5.27 ± 0.05	-5.23 ± 0.05

[a]The minimum helium ionization case assumes $x(\mathrm{He}^{+2})_{WIM} = 0$. We prefer this assumption over the maximum helium ionization case.

[b]The maximum helium ionization case assumes $x(\mathrm{He}^{+2})_{WIM} = 1 - x(\mathrm{He}^{+})_{WIM}$.

[c]The values of η_{WIM} are derived assuming $0.67 \lesssim x(\mathrm{H}^+)_{WIM} \lesssim 1.0$ and $x(\mathrm{He}^+)_{WIM} \lesssim 0.27\, x(\mathrm{H}^+)_{WIM}$. The uncertainties quoted encompass the range of values derived using these constraints and the assumptions regarding $x(\mathrm{He}^{+2})_{WIM}$ appropriate for each model.

[d]These quantities refer only to warm gas, including the WNM and WIM. They exclude ionized gas associated with

the HIM.

[e]The quantities with the subscript “Total” include contributions from both warm and hot gas, i.e., they include ionized gas associated with the HIM.

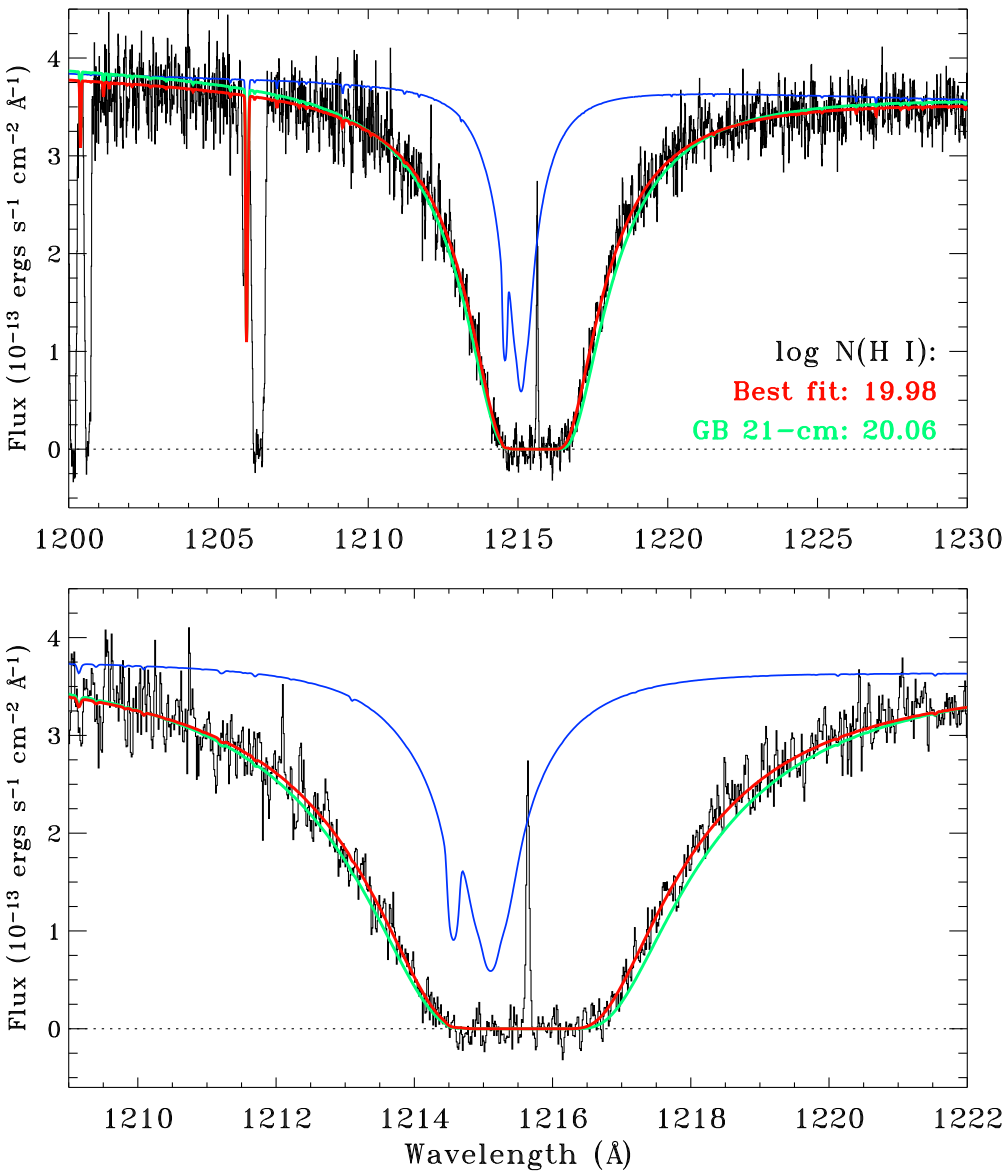

Fig. 1.— Two views of the STIS E140M spectrum of the Lyman-α absorption profile toward vZ 1128. Both stellar and interstellar absorption contribute to this profile. The estimated stellar profile is shown as the thin blue line and has been shifted to $v_{LSR} = -145$ km s^{-1} to match the observed positions of stellar absorption lines in the STIS spectrum. The best fit to the interstellar and stellar absorption profile is shown in red, corresponding to an interstellar column density $\log N(\mathrm{H\ I}) = 19.98 \pm 0.03$. The green line shows the best fit profile adopting the H I column density derived from Green Bank 140-ft telescope observations of 21-cm emission in this direction, $\log N(\mathrm{H\ I}) = 20.04 \pm 0.01$ (see Paper I). The sharp emission line in the center of the Lyman-α absorption trough is geocoronal emission. The strong stellar line near 1206 Å is stellar Si III.

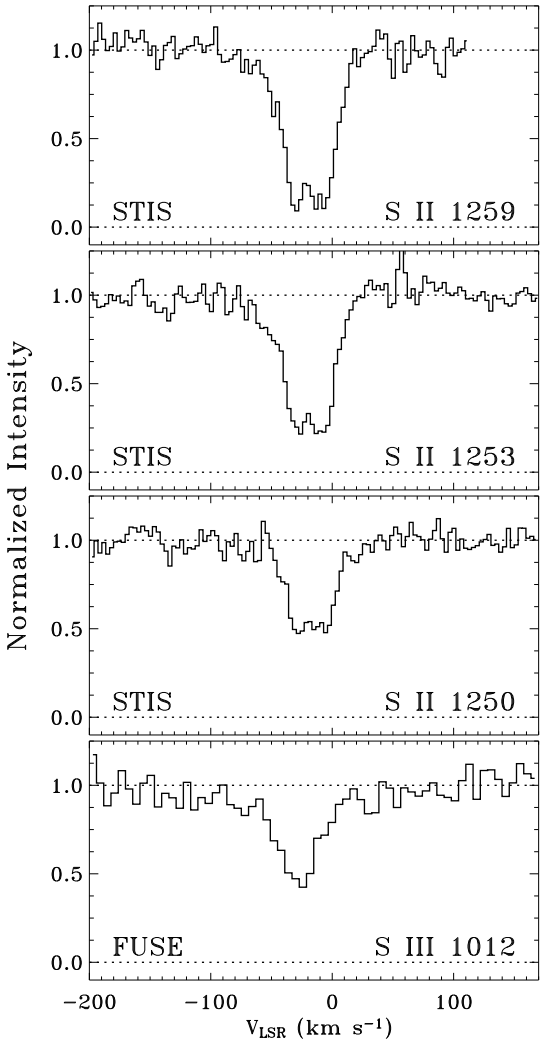

Fig. 2.— Absorption line profiles of S II $\lambda 1250.584, 1253.811$, and 1259.519 from STIS E140M observations and S III $\lambda 1012.495$ from *FUSE* (see Paper I). We suggested in Paper I that the material at $v_{\rm LSR} \approx -30$ km s^{-1} was likely associated with the Galactic thick disk given the higher degree of ionization compared with the material at $v_{\rm LSR} \approx -4$ km s^{-1}. The STIS data have a resolution of ~ 6.5 km s^{-1}, while the *FUSE* data have a resolution ~ 20 km s^{-1}.

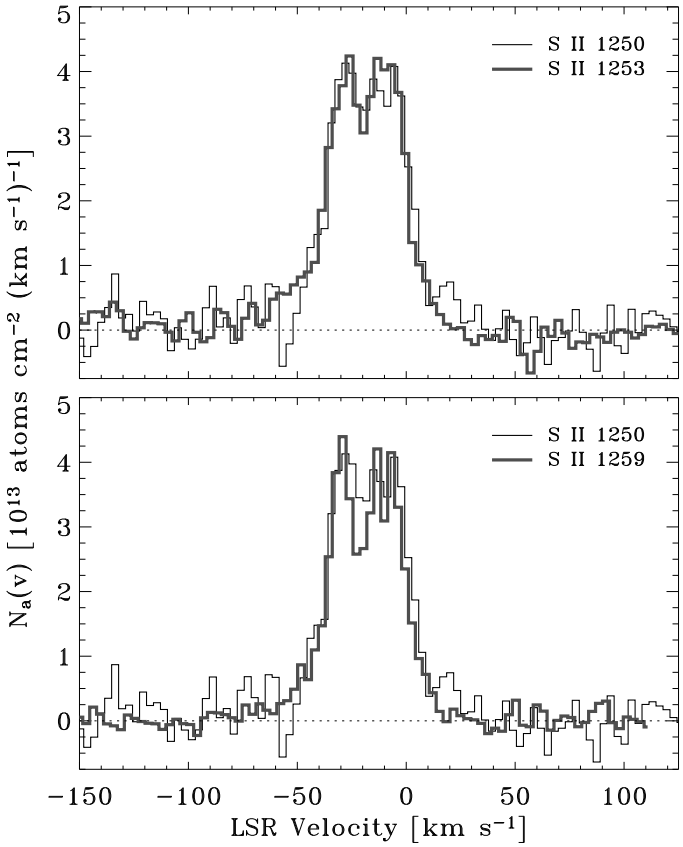

Fig. 3.— Comparison of the apparent column density profiles for S II $\lambda 1250.584, 1253.811$, and 1259.519 from STIS E140M observations. The weaker two lines (at 1250.584 and 1253.811 Å) are compared in the top panel; the strongest line (1259.519 Å) is compared with the weakest in the lower panel. The lack of agreement between these profiles indicates the stronger line contains a small amount of unresolved saturated structure.